Chapter

Corneal Pachymetry and Endothelial Microscopy by Slit-Lamp

Silvia Tavazzi, Alessandra Parodi, Sara Colciago, Gabriele Nigrotti, Simone Borghesi and Fabrizio Zeri

Abstract

A slit-lamp biomicroscope Visionix VX75 has been equipped with a high-resolution digital sensor. A specular reflection technique at an angular magnification of 36× performed by the slit-lamp biomicroscope is used to develop a procedure to (i) measure the thickness of the human cornea by measuring the distance between the two reflections of its anterior and posterior surfaces and (ii) capture suitable images for morphometric analyses of the corneal endothelium's cell mosaic. The examples of morphometric analysis of these images are reported. The biases due to the dioptric power of the anterior surface of the cornea, the oblique observation, and the asymmetry of the digital biomicroscope are discussed. These biases can be corrected by a specific calibration.

Keywords: slit-lamp biomicroscope, pachymetry, endothelial microscopy, specular reflection, morphometric analysis

1. Introduction

The slit-lamp biomicroscope is an instrument widely used by ophthalmologists and optometrists to observe the anterior segment of the eye. The instrument is composed by two main components: an illumination system, the slit-lamp, and an observation system, the biomicroscope. They can be set up in different configurations allowing several types of illumination techniques. One of these is the specular reflection: the examiner directs the incident light toward the eye with angle of incidence α on the anterior surface of the cornea, then sets the angle between the illumination system and the biomicroscope at 2α, and observes the bright reflection on the anterior surface through the biomicroscope. Usually the angle 2α is relatively high, ranging from 40 to 70°. The intense reflection is due to the change of refractive index between the air and the anterior surface of the cornea. A digital camera coupled with the right or left eyepiece tube can be used to capture images. Part of the light reaching the observation system is deviated by a beam splitter toward a converging lens, which allows the formation of a real image on the plane of the digital sensor.

The configuration of the specular reflection can also be used to observe the reflection from the posterior surface of the cornea (endothelium) due to the change

of refractive index between the corneal endothelium and aqueous humor. However, this second reflection is much less evident than the previous one because of the smaller variation of refractive index between the two adjacent components. To observe the posterior reflection, light coming from the illumination system is focalized on the posterior surface and generates an image of the illuminated slit. The correct focus may be reached through the eyepieces' view, and a real image is detected on the digital sensor. In this configuration, only the posterior corneal surface (within the depth of field of the system) is in focus. This surface is optically conjugated with the plane of the sensor. A sort of slit image is also formed on the anterior surface of the cornea, but it is not a perfectly focused image of the slit and, consequently, neither is the resulting image on the sensor of the biomicroscope.

When a relatively narrow slit is used, the distance on the sensor between the in-focus image and the other image of the slit (formed by reflected beams from posterior and anterior surfaces, respectively) can be used to deduce the thickness of the cornea (pachymetry). A relatively narrow beam is recommended to reduce uncertainty in finding the distance between the two surfaces, i.e., the corneal thickness. Corneal pachymetry is a technique used in clinical practice for monitoring different conditions such as the progress of corneal diseases, to evaluate suitable patients before refractive surgery, and to determine intraocular pressure. During routine examination by slit-lamp biomicroscope, corneal thickness can also be measured by considering the apparent thickness of the optical section of the cornea [1]. Other methods are ultrasound pachymetry, optical coherence tomography, Scheimpflug imaging [2–15].

With a larger slit, the endothelium cell mosaic can be seen adjacent to the region of the intense light reflection from the anterior surface. The corneal endothelium is a cell monolayer laying on the posterior surface of the cornea. It regulates the transport of solutes and water across the interface between the cornea and anterior chamber of the eye. Pathologies such as the narrow-angle glaucoma, iritis, and corneal dystrophies can change the shape and size of the endothelial cells and their number per unit area, as well as trauma, aging, intraocular surgery, drugs, and wear of contact lenses [16–20]. A significant loss of cells is typically accompanied by an increase in the variability of cell size (polymegethism) and shape (polymorphism). Endothelium analysis is often carried out by automatic instruments, while the analysis by a digital slit-lamp biomicroscope is less expensive and allows to observe any specific region of interest of the cornea, so that a more complete characterization of the endothelium can be achieved. However, the common cell recognition methods are often not applicable to images taken by a slit-lamp biomicroscope. The main problem is typically the lack of information in some parts of the cells' borders [21]. A recent method was reported in 2016 allowing an improved cell recognition and morphometric analysis [22]. It was applied to a Takagi 700 GL LED biomicroscope equipped with TD-10 digital camera.

This chapter describes the results obtained by a Visionix VX75 slit-lamp biomicroscope equipped with a high-resolution digital sensor. We captured in vivo images of the two reflections from anterior and posterior corneal surfaces to deduce corneal thickness (pachymetry). We took images of the corneal endothelium with larger slits. They show the typical cell mosaic, and they are suitable for morphometric analysis. The effects of the dioptric power of the anterior surface of the cornea, of the oblique observation, and of the asymmetry of the digital biomicroscope on morphometric analysis are also discussed. The effects of these potential systematic errors can be greatly reduced by a preliminary calibration.

2. Methods

A Visionix VX75 slit-lamp biomicroscope equipped with a digital sensor Matrix Vision (sensor size, 2464 × 2056 pixels; pixel size, 3.45 × 3.45 μm^2; maximum number of frames per second, 35) was used with an angular magnification setting of the biomicroscope equal to 36×. A dedicated software was developed to take images through this sensor. A live digital magnification controlled by the operator was also applied to facilitate image acquisition. Images of the illuminated slit on the posterior surface of human corneas were taken in vivo both in the case of relatively narrow slits (for pachymetry analyses) and in the case of larger slits (for endothelial microcopy analyses). A sequence of MATLAB functions was created for the analysis of the images.

3. Slit-lamp biomicroscope corneal pachymetry

Figure 1 shows an example of image of the two reflections from the anterior corneal surface (slit image not perfectly in focus) and from the posterior surface (slit image in focus) taken at 36× on the central portion of the cornea of a young adult.

General equations on the relationship between true corneal thickness t and apparent corneal thickness s observed by a biomicroscope at oblique observation are reported in the literature [23, 24]. These equations can also be applied to the specific configuration of specular reflection. In this case, s is the lateral distance between the two reflections from anterior and posterior corneal surfaces, such as those of **Figure 1**. **Figure 2** is inspired by a figure reported in Brennan et al. [23], from which the following Eqs. (1)–(3) are also deduced:

$$\frac{R}{t} \sim \frac{R}{s}(c_1 + c_2)\cos\phi_2 + \frac{k_1 + k_2}{c_1 + c_2} - \frac{1}{2}(c_1 - c_2)\tan(\phi_2) \tag{1}$$

where t is the true thickness, s is the apparent thickness (viz., the distance between the two reflections in the case of specular reflection), and R is the

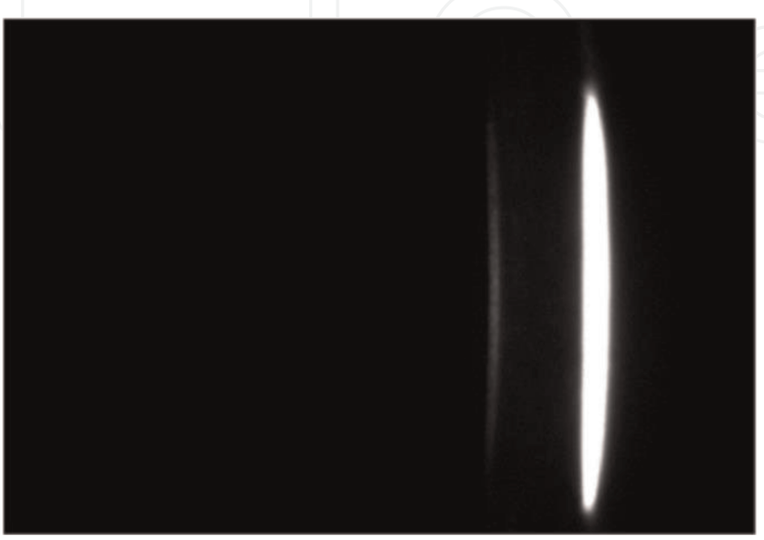

Figure 1.
Example of the two reflections from the anterior corneal surface (slit image on the right, not perfectly in focus) and from the posterior surface (slit image on the left, in focus) taken on the central portion of the cornea of a young adult by a Visionix VX75 slit-lamp biomicroscope at 36×.

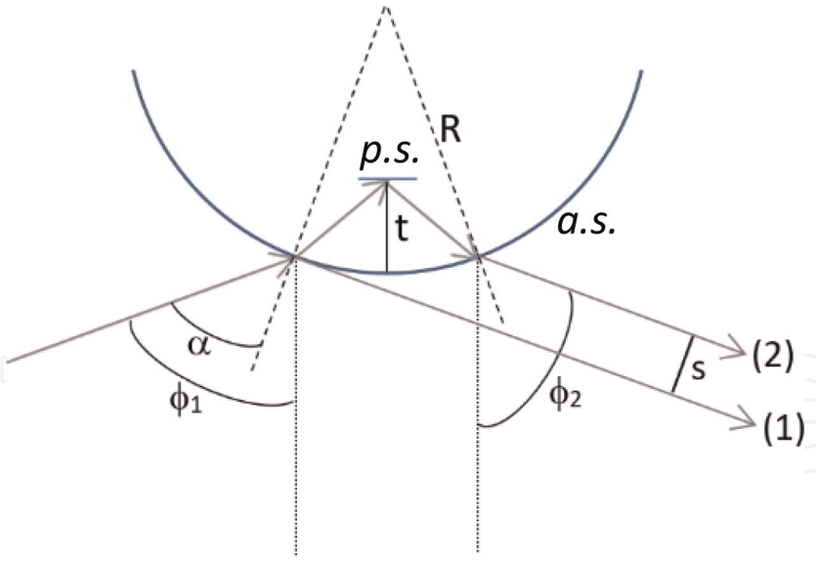

Figure 2.
Scheme showing apparent thickness s *and true thickness* t *of a sample (e.g., the human cornea) with spherical anterior surface (curvature radius R) as reported by Brennan et al. [23, 24]. ϕ_1 and ϕ_2 are the angles that appear in Eqs. (1)–(3) [23]. Labels* p.s. *and* a.s. *indicate the posterior surface and the anterior surface, respectively. Labels (1) and (2) indicate the rays of light reflected from the anterior and posterior surfaces, respectively, in the configuration of specular reflection.*

curvature radius of the anterior surface. Angles ϕ_1 and ϕ_2 are shown in **Figure 2**; c_j and k_j are

$$c_j = \frac{1}{\sqrt{\frac{n^2}{\sin^2(\phi_j)} - 1}} \tag{2}$$

$$k_j = c_j + \frac{c_j^3}{2} - \frac{c_j^2 n^2}{\tan\left(\phi_j\right)\sin^2\left(\phi_j\right)} \tag{3}$$

where j = 1, 2 and n is the cornea refractive index (n = 1.376 [25]).

In the specific case of specular reflection, angles ϕ_1 and ϕ_2 are equal ($\phi_1 = \phi_2 = \phi$) and Eq. (1) can be written as

$$\frac{R}{t} \sim \frac{R}{s}\left(\frac{2}{\sqrt{\frac{n^2}{\sin^2(\phi)} - 1}}\right) cos\phi + 1 + \frac{1}{2\left[\frac{n^2}{\sin^2(\phi)} - 1\right]} - \frac{n^2}{\tan(\phi)\sin^2(\phi)\sqrt{\frac{n^2}{\sin^2(\phi)} - 1}} \tag{4}$$

In the limit case of a flat sample ($R \to \infty$), Eq. (4) reduces to

$$t = \frac{s}{2\ \cos(\alpha)\ \tan\left(arcsin\left(\frac{sin(\alpha)}{n}\right)\right)} \tag{5}$$

By measuring the distance s between the two reflections observed in the image (e.g., as in **Figure 1**), from Eq. (4), we deduce the true corneal thickness t. However, this procedure contains a systematic error. The image of **Figure 1** was taken with an angular magnification setting of the biomicroscope equal to 36× and the angle between the axis of the illumination system, and the axis of the biomicroscope was fixed at 45°. Therefore, to a first approximation, the angle 2° can be set to be

45°. However, this assumption contains a systematic error due to the asymmetry of digital biomicroscopes [24]. Indeed, the sensor of a digital biomicroscope is positioned either at the right or at the left eyepiece of the biomicroscope (left side in the case of the Visionix VX75 biomicroscope). The sample is typically slightly rotated by an angle γ to direct the light beam into the correct channel of the biomicroscope and reach the sensor, as discussed in Ref. [24]. For the Visionix VX75 biomicroscope, γ was measured to be about 2.5°. During the acquisition of the image reported in **Figure 1**, the illumination system was positioned to the right of the examiner and the biomicroscope to the left. The digital sensor was placed on the left eyepiece of the biomicroscope, so that the true angle between the incident beam and the beam directed to the sensor is not the angle 2ϕ between illumination and biomicroscope, but it is equal to $2(\phi + \gamma)$. Therefore, due to this asymmetry of the digital biomicroscope, ϕ_1 and ϕ_2 in **Figure 2** and ϕ in Eq. (4) must be replaced with $(\phi + \gamma)$, i.e., about 25° in the considered case. Considering this aspect, the measure of s by the slit-lamp biomicroscope determines the thickness t. As discussed in Section 5, the bias in this procedure can be corrected by a system calibration.

4. Slit-lamp biomicroscope endothelial microscopy

Figure 3 shows few examples of images of the corneal endothelium of different subjects taken through the 36× objective. A different view of the corneal endothelium of a young adult is reported in **Figure 4**. The x and y coordinates corresponding to the image plane are shown on two axes. The third axis (z) shows the luminance of the image at each pixel.

Corneal endothelium can be described by endothelial cell density (ECD), cell hexagonality (HEX), and coefficient of variation (CoV). ECD is the number of cells per unit area. HEX is the percentage of cells with six nearest-neighbor cells, also defined as the percentage of six-sided cells. CoV is the ratio between standard deviation and mean value of the areas of the cells. As already mentioned, a significant loss of cells due to specific pathologies causes a decrease of ECD, and it is typically accompanied by an increase in the variability of cell size (polymegethism) and shape (polymorphism). However, the correlation between ECD and the other two parameters is typically poor because the measured ECD value (in contrast to HEX and CoV) depends on factors such as (i) the magnification of the images produced by the anterior surface of the cornea, which can vary from subject to subject, and (ii) the intrinsic cell size, which may also vary from subject to subject, even in the presence of perfectly regular hexagonal mosaics. On the contrary, a negative correlation is expected between CoV and HEX [26–30]: the higher the polymegethism (relatively high CoV), the higher the polymorphism (relatively low HEX).

ECD, HEX, and CoV can be deduced from images such as those reported in **Figures 3** and **4**. The computation of those parameters on a sample involves a lengthy counting process, if manually done by an operator. An automated way of determining such parameters is therefore desirable. The starting point is capturing a good quality image of the endothelium, inside which the operator can select a region of interest, preferably containing a few hundreds of cells (to get a statistically significant sample [31]) with sharp details uniformly illuminated. An automatized sequence of MATLAB functions acting on this region of interest was created. The purpose is, at first, to automatically detect cells' boundaries as accurately as possible and then to compute relevant cells' statistics from them. The following figures highlight some intermediate steps of the procedure. **Figure 5** shows the selection of the area of interest while **Figure 6** the obtained partition of the region of interest

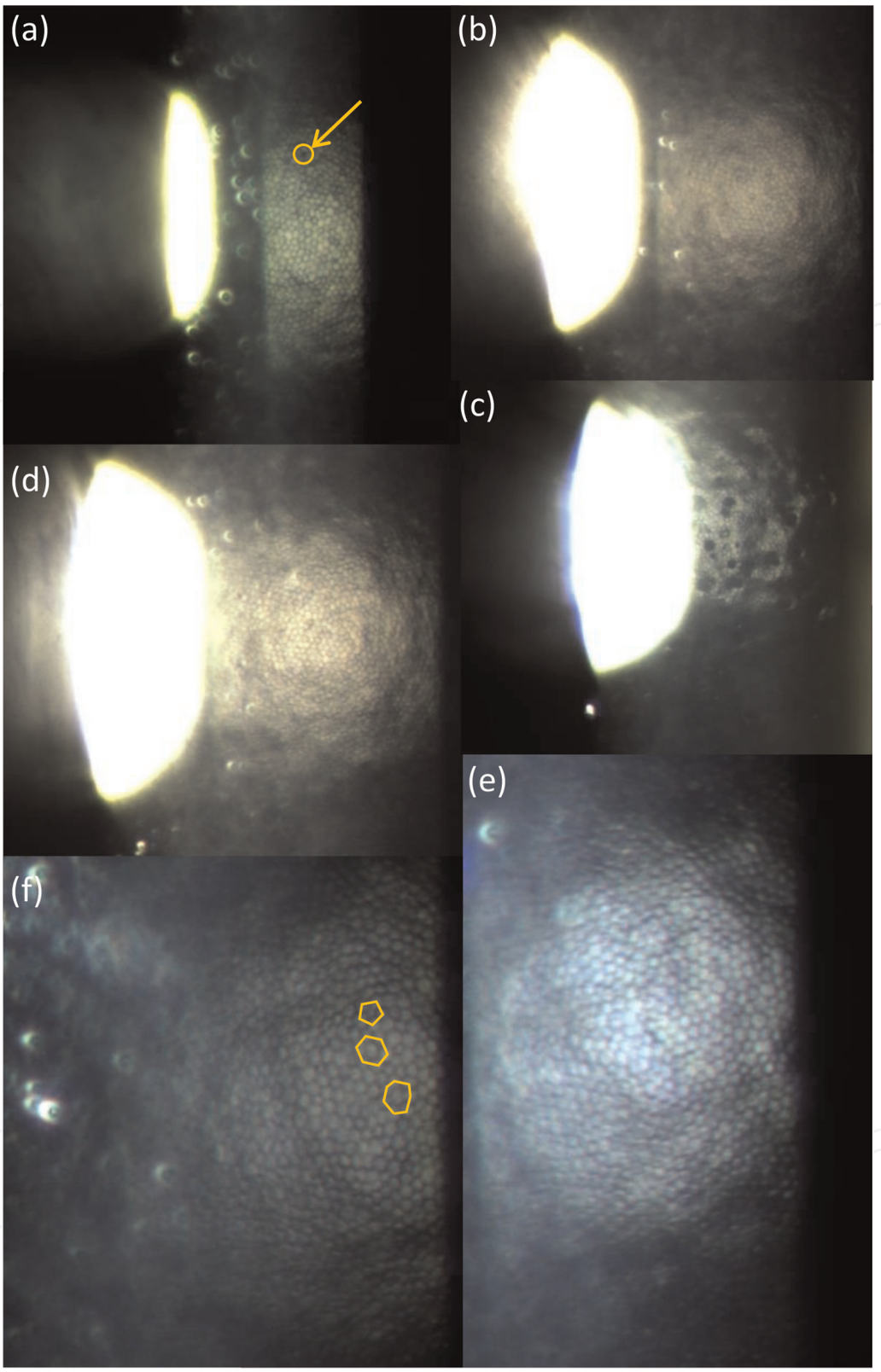

Figure 3.
Examples of images (a–d) and examples of enlarged portions of images (e, f) of the corneal endothelium of different subjects taken by a Visionix VX75 slit-lamp biomicroscope at 36×. In (a), a circle with an arrow indicates how a typical endothelial bleb appears. In (c), several endothelial guttae can be observed. In (f), a hexagon shows the typical hexagonal packing of regular mosaics of endothelial cells where each cell has six nearest neighbors. The other two closed polygons highlight 5 and 7 nearest-neighbor cells, respectively.

along cells' boundaries. Finally, in **Figure 7** we display the histograms of cells' area and the histograms of cells' gonality. The gonality of a cell is defined as the number of cells that are its nearest neighbors; sometimes it is also defined as the number of

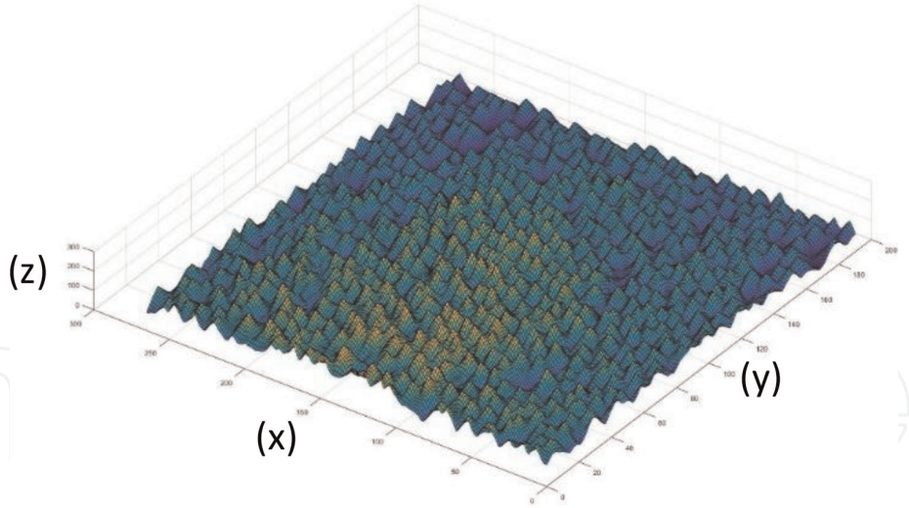

Figure 4.
View of a portion of the cell mosaic of the corneal endothelium of a young adult taken by a Visionix VX75 slit-lamp biomicroscope at 36×. The x and y coordinates corresponding to the image plane are shown on two axes. The third axis (z) shows the luminance of the image.

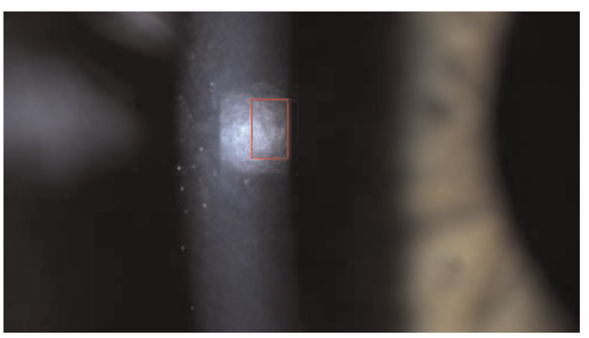

Figure 5.
Selection of the region of interest on the image of a corneal endothelium taken by slit-lamp biomicroscope.

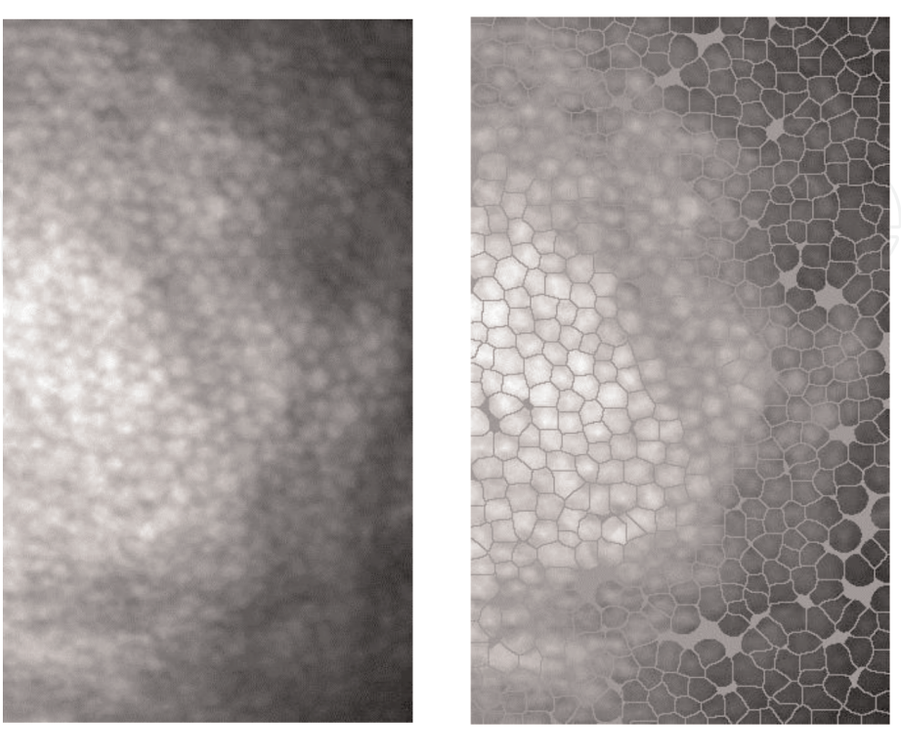

Figure 6.
Region of interest zoomed and partitioned along cells' boundaries.

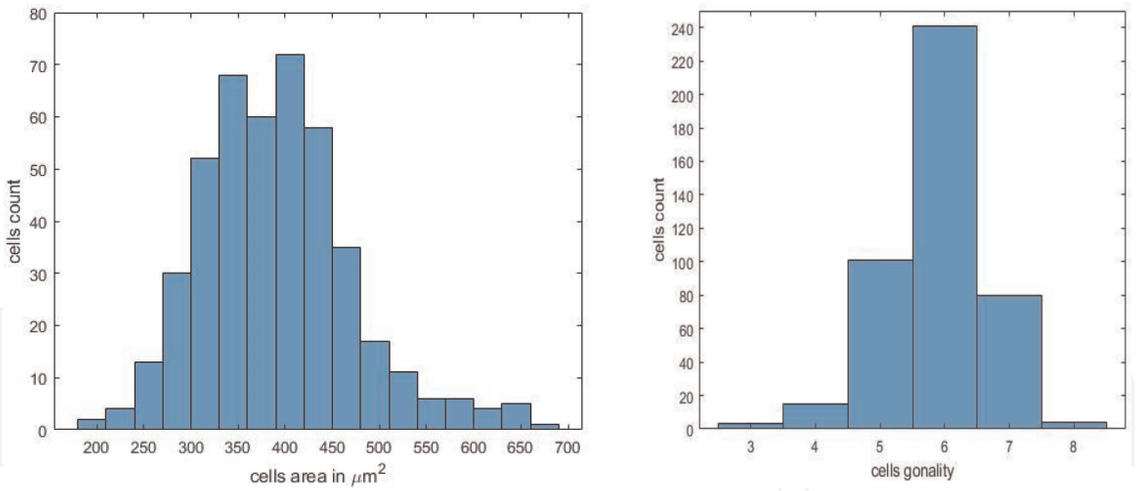

Figure 7.
Cells' area distribution (left) and cells' gonality distribution (right).

sides of the cell. In the specific example of **Figures 5–7**, MATLAB functions selected 444 cells for data computations.

A few aspects must be considered, for a quantitative evaluation of the parameters ECD, HEX, and CoV: firstly, the effects on ECD of the image magnification due to the dioptric power of the corneal anterior surface. ECD can be evaluated by the ratio N/A, where N is the number of recognized cells in a selected area A. The dioptric power of the corneal anterior surface induces a magnification on the sensor of this area, thus requiring the correction of the measured density to obtain the true value of ECD. In addition to the magnification produced by the anterior surface of the cornea, the angle of observation is another aspect that influences the area of the image [22]. The posterior corneal surface is indicated by a segment in **Figure 2** with label *p.s.* Its image is captured along the direction indicated by the ray (2) in the same figure. The larger the angle of observation, the larger the portion of internal surface projected onto the plane of the sensor. In other words, the cells in the image are narrowed along one direction. If not accounted for, this shrinkage is responsible for the increase of the measured cell density on the sensor due to the larger angle of observation. Moreover, the correction for such an angle presents the same issues discussed above, concerning the asymmetry of digital biomicroscopes. During the acquisition of the images reported in **Figures 3** and **4**, the illumination system was positioned on the left and the biomicroscope on the right. The digital sensor was on the left eyepiece of the biomicroscope, so that the true angle of the incident beam and the true angle of observation are not ϕ, but $(\phi - \gamma)$, i.e., about 20° in the considered case. As discussed in Section 5, a calibration with a suitable sample corrects these errors. Interestingly, the inaccuracy induced by the dioptric power of the anterior corneal surface, by the oblique observation, and by the asymmetry of the digital biomicroscope affects only ECD measurements. Unlike ECD, the other two parameters, HEX and CoV, are not influenced by the magnification factor because they are not influenced by possible errors in the measurement of the selected area A.

5. Reference standard sample for calibration

By what is discussed in the previous section, a calibration is recommended before a quantitative analysis of the corneal thickness (Section 3) and the endothelial cell density (Section 4). For this purpose, images of a planar reference grid

should be taken at the desired angular magnification setting of the biomicroscope. The linear magnification of the real image on the sensor can be computed as the ratio between the size of the image of the elements of the reference grid and the size of the reference grid itself.

While the calibration through a planar grid can correct for errors induced by the lateral shrinkage of the image caused by the oblique observation and the biomicroscope's asymmetry, it will not account for issues related to the dioptric power of cornea's anterior surface. One further calibration employing a reference lens, such as the standard samples proposed in Refs. [22, 30], is used to counterbalance this effect. They were developed to reproduce the cornea with its typical shape and the endothelium with cell sizes of approximately 20 μm in diameter. These standard samples consist of a layer of polystyrene beads of calibrated diameter deposited on the internal surface of a poly(methyl-methacrylate) lens simulating the cornea. Images of the polystyrene beads must be taken in the same configurations and at the same angle of observation as in vivo pachymetry or endothelial analyses. The comparison between expected thickness and expected bead density and measured values determines the corrective factor for in vivo thickness and ECD measurements. Concerning the expected bead density corresponding to a hexagonal bead packing, the number of beads per unit area (density δ of beads) can be calculated as

$$\delta = \frac{1}{2\sqrt{3}r^2} \tag{6}$$

where r is the radius of each bead. The beads proposed in Ref. [22] have radius, r = 10.14 μm, so that the expected density δ can be calculated by Eq. (6) to be 2808 mm^{-2}.

6. In vivo results

After the calibration, corneal central thickness, ECD, HEX, and CoV were measured in vivo in a small group of ten healthy subjects (age: 20–30 years). They were enrolled on a voluntary basis following the Declaration of Helsinki. Inclusion criteria were the absence of any known corneal pathology and to be between the ages of 20 and 30 years.

The analysis was performed on the right eye of each subject, each of whom was asked to look at a far target during the image acquisitions. Images were taken with a relatively narrow slit (pachymetry) and with a larger slit to observe the endothelial mosaic (endothelial microscopy). Images were taken in the central portion of the cornea, at a distance lower than 2 mm from the center of the pupil.

Although the group is small and it might not therefore account for a reliable statistical analysis, the mean (±standard deviation) of the ten measured values was calculated. The mean central corneal thickness was found to be 502 μm (± 73 μm). The results are in reasonable agreement with data reported in the literature. For example, Olsen and Ehlers reported a mean central corneal thickness of (515 ± 33) μm calculated on 115 eyes between 10 and 90 years [32]. Doughty and Zaman [33] reported a value of 534 μm for "normal" human central corneal thickness. Wirbelauer et al. [34] found (541 ± 43) μm for the mean central corneal thickness of 108 subjects (age range: 25–87 years). Altay et al. [35] reported mean values on 137 subjects (age range: 18–64 years) equal to (522 ± 34), (543 ± 34), and (538 ± 35) μm, measured by Scheimpflug camera, specular microscopy, and ultrasound pachymetry, respectively. Compared to other techniques, the measurement

of corneal thickness with the slit-lamp biomicroscope adds no extra costs for the clinicians, who routinely use this instrument. It should be noted that the method of specular reflection can only be used on subjects with healthy corneas. Keratoconus, corneal opacities, and other irregularities may distort the light beam or dim the endothelium reflex beyond acceptable levels. This disadvantage is also relevant for other techniques such as the systems based on Scheimpflug camera.

Regarding the endothelial mosaic, the mean (± standard deviation) of ten measured values yielded 2671 mm^{-2} (± 133 mm^{-2}) for ECD, 46% (± 5%) for HEX, and 31% (± 3%) for CoV. The results are in reasonable agreement with data in the literature. Variations of ECD, HEX, and CoV are expected due to several factors such as hypoxia [36] and age [20]. If considering only in vivo measurements and relatively young subjects, values of mean central ECD reported in the literature can be found in the range of 2600–3000 mm^{-2} [19, 20, 37, 38]. Central HEX measured by Wiffen et al. [19] and Zheng et al. [38] is (63 ± 7) and (49 ± 13)%. Normal CoV range is considered 20–30% [20]. As already mentioned in the introduction, endothelium analysis is often carried out by automatic instruments; however, the analysis by a digital slit-lamp biomicroscope is less expensive and allows to observe any specific region of interest of the cornea in the center and in the periphery.

7. Conclusions

A high-resolution digital sensor was applied to a Visionix VX75 slit-lamp biomicroscope. A software for image acquisition, including a live digital magnification facility, was developed. A procedure is here proposed to use the apparatus in configuration of specular reflection for pachymetry analyses and for endothelial microscopy analysis at angular magnification 36×. Images are suitable for morphometric analysis of the cell mosaic of corneal endothelium, and an automatized sequence for image analysis was developed. The effects of (i) the dioptric power of the anterior corneal surface, (ii) oblique observation, and (iii) intrinsic asymmetry of digital biomicroscopes are discussed. For a quantitative analysis of corneal thickness and endothelial cell density, these effects must be taken into consideration and can be corrected by a procedure of calibration. On the contrary, the other two parameters (endothelium cell hexagonality and coefficient of variation of the cell areas) are not influenced by these aspects.

Acknowledgements

Visionix is acknowledged for supplying a Visionix VX75 slit-lamp biomicroscope.

Conflict of interest

The authors declare no conflicts of interest.

Author details

Silvia Tavazzi[1,2*], Alessandra Parodi[1], Sara Colciago[1], Gabriele Nigrotti[2], Simone Borghesi[3] and Fabrizio Zeri[1,2,4]

1 Department of Materials Science, University of Milano Bicocca, Milan, Italy

2 COMiB Research Centre in Optics and Optometry, University of Milano Bicocca, Milan, Italy

3 Department of Mathematics and Applications, University of Milano Bicocca, Milan, Italy

4 School of Life and Health Sciences, Aston University, Birmingham, UK

*Address all correspondence to: silvia.tavazzi@unimib.it

References

[1] Agarwal T, Bhartiya S, Dada T, Panda A, Jhanji V, Yu M. Agreement of corneal thickness measurement using slit-lamp and ultrasound pachymetry. Eye & Contact Lens: Science & Clinical Practice. 2012;**38**:231-233

[2] Hitzenberger CK. Measurement of corneal thickness by low coherence interferometry. Applied Optics. 1992;**31**: 6637-6642

[3] Hitzenberger CK, Baumgartner A, Drexler W, Fercher AF. Interferometric measurement of corneal thickness with micrometer precision. American Journal of Ophthalmology. 1994;**118**:468-476

[4] Drexler W, Baumgartner A, Findl O, Hitzenberger CK, Sattmann H, Fercher AF. Submicrometer precision biometry of the anterior segment of the human eye. Investigative Ophthalmology & Visual Science. 1997;**38**:1304-1313

[5] Böhnke M, Chavanne P, Gianotti R, Salathé RP. Continuous noncontact corneal pachymetry with a high speed reflectometer. Journal of Refractive Surgery. 1998;**14**:140-146

[6] Waelti R, Böhnke M, Gianotti R, Bonvin P, Ballif JJ, Dalathé RP. Rapid and precise in vivo measurement of human corneal thickness with optical low-coherence reflectometry in normal human eyes. Journal of Biomedical Optics. 1998;**3**:253-258

[7] Huang D, Wang I, Lin CP, Puliafito CA, Fujimoto JG. Micron-resolution ranging of cornea anterior chamber by optical reflectometry. Lasers in Surgery and Medicine. 1991;**11**:419-425

[8] Izatt JA, Hee MR, Swanson EA, Lin CP, Huang D, Schuman JS, et al. Micrometer-scale resolution imaging of the anterior eye in vivo with optical coherence tomography. Archives of Ophthalmology. 1994;**112**:1584-1589

[9] Fujioka M, Nakamura M, Tatsumi Y, Kusuhara A, Maeda H, Negi A. Comparison of Pentacam Scheimpflug camera with ultrasound pachymetry and noncontact specular microscopy in measuring central corneal thickness. Current Eye Research. 2007;**32**:89-94

[10] Uçakhan OO, Ozkan M, Kanpolat A. Corneal thickness measurements in normal and keratoconic eyes: Pentacam comprehensive eye scanner versus noncontact specular microscopy and ultrasound pachymetry. Journal of Cataract and Refractive Surgery. 2006; **32**:970-977

[11] Kawana K, Tokunaga T, Miyata K, Okamoto F, Kiuchi T, Oshika T. Comparison of corneal thickness measurements using Orbscan II, non-contact specular microscopy, and ultrasonic pachymetry in eyes after laser in situ keratomileusis. The British Journal of Ophthalmology. 2004;**88**: 466-468

[12] Borrego-Sanz L, Sáenz-Francés F, Bermudez-Vallecilla M, Morales-Fernández L, Martinez-de-la Casa JM, Santos-Bueso E, et al. Agreement between central corneal thickness measured using Pentacam, ultrasound pachymetry, specular microscopy and optic biometer lenstar LS 900 and influence of ıntraocular pressure. Ophthalmologica. 2014;**231**:226-235

[13] De Bernardo M, Borelli M, Mariniello M, Lanza M, Rosa N. Pentacamvs SP3000P specular microscopy in measuring corneal thickness. Contact Lens & Anterior Eye. 2015;**38**:21-27

[14] Sanchis-Gimeno JA, Herrera M, Lleo-Perez A, Alonso L, Rahhal MS, Martinez-Soriano F. Quantitative anatomical differences in central corneal thickness values determined with scanning-slit corneal topography and

noncontact specular microscopy. Cornea. 2006;**25**:203-205

[15] Tai LY, Khaw KW, Ng CM, Subrayan V. Central corneal thickness measurements with different imaging devices and ultrasound pachymetry. Cornea. 2013;**32**:766-771

[16] Waring GO, Bourne WM, Edelhauser HF, Kenion KR. The corneal endothelium: Normal and pathologic structure and function. Ophthalmology. 1982;**89**:531-590

[17] MacRae SM, Matsuta M, Shellans S, Rich LF. The effects of hard and soft contact lenses on the corneal endothelium. American Journal of Ophthalmology. 1986;**102**:50-57

[18] Schoessler JP. Contact lens wear and the corneal endothelium. Journal of the American Optometric Association. 1987; **58**:804-810

[19] Wiffen SJ, Hodge DO, Bourne WM. The effect of contact lens wear on the central and peripheral corneal endothelium. Cornea. 2000;**19**:47-51

[20] McCarey BE, Edelhauser HF, Lynn MJ. Review of corneal endothelial specular microscopy for FDA clinical trials of refractive procedures, surgical devices and new intraocular drugs and solutions. Cornea. 2008;**27**:1-16

[21] Comanducci D, Colombo C. Vision-based magnification of corneal endothelium frames. In: Proceedings of the 9th International Conference on Computer Vision Systems ICVS'13; St. Petersburg, Russia; 2013. pp. 52-61

[22] Ferraro L, Cozza F, Scialdone A, Borghesi A, Tavazzi S. Morphometric analyses by a new slit-lamp endothelial biomicroscope. Cornea. 2016;**35**: 1347-1354

[23] Brennan NA, Smith G, Macdonald JA, Bruce AS. Theoretical principles of optical pachymetry. Ophthalmic & Physiological Optics. 1989;**9**:247-254

[24] Marelli A, De Vita IR, Cozza F, Tavazzi S. Criticality of the measurement of corneal thickness in specular reflection by digital biomicroscope. Contact Lens & Anterior Eye. 2018;**41**:531-537

[25] Patel S. Refractive index of the mammalian cornea and its influence during pachometry. Ophthalmic & Physiological Optics. 1987;**7**:503-506

[26] Schoessler J, Woloschak M. Corneal endothelium in veteran PMMA contact lenses wearers. International Contact Lens Clinic. 1981;**8**:19-25

[27] Rao GN, Lohman LE, Aquavella JV. Cell size-shape relationship in corneal endothelium. Investigative Ophthalmology & Visual Science. 1982; **22**:271-274

[28] Suda T. Mosaic pattern changes in human corneal endothelium with age. Japanese Journal of Ophthalmology. 1984;**28**:331-338

[29] Orsborn GN, Schoessler JP. Corneal endothelial polymegathism after the extended wear of rigid gas-permeable contact lenses. American Journal of Optometry and Physiological Optics. 1988;**65**:84-90

[30] Tufo S, Prazzoli E, Ferraro L, Cozza F, Borghesi A, Tavazzi S. Variable-size bead layer as standard reference for endothelial microscopes. Cornea. 2017; **36**:236-240

[31] Doughty MJ, Fonn D, Nguyen KT. Assessment of the reliability of calculations of the coefficients of variations for normal and polymegethous human corneal endothelium. Optometry and Vision Science. 1993;**70**:759-770

[32] Olsen T, Ehlers N. The thickness of the human cornea as determined by a specular method. Acta Ophthalmologica. 1984;**62**:859-871

[33] Doughty MJ, Zaman ML. Human corneal thickness and its impact on intraocular pressure measures: A review and meta-analysis approach. Survey of Ophthalmology. 2000;**44**:367-408

[34] Wirbelauer C, Scholz C, Hoerauf H, Pham DT, Laqua H, Birngruber R. Noncontact corneal pachymetry with slit lamp-adapted optical coherence tomography. American Journal of Ophthalmology. 2002;**133**:444-450

[35] Altay Y, Balta O, Demirok G, Burcu A, Balta OB, Ornek F. Agreement between corneal thickness measurements using Pentacam Scheimpflug camera, noncontact specular microscopy, and ultrasonographic pachymetry in diabetic patients. Current Eye Research. 2017;**42**:187-194

[36] Polse KA, Brand RJ, Cohen SR, Guillon M. Hypoxic effects on corneal morphology and function. Investigative Ophthalmology & Visual Science. 1990; **31**:1542-1554

[37] Amann J, Holley GP, Lee SB, et al. Increased endothelial cell density in the paracentral and peripheral regions of the human cornea. American Journal of Ophthalmology. 2003;**135**:584-590

[38] Zheng T, Le Q, Hong J, et al. Comparison of human corneal cell density by age and corneal location: An in vivo confocal microscopy study. BMC Ophthalmology. 2016;**16**:109